ACS SENSORS

ACS Editors' Choice

Article

pubs.acs.org/acssensors

# Evaluating Cellular Drug Uptake with Fluorescent Sensor Proteins

Silvia Scarabelli,[†,‡] Kui Thong Tan,[†,‡,#] Rudolf Griss,[†,‡,¶] Ruud Hovius,[†,‡] Pier Luca D'Alessandro,[§] Thomas Vorherr,[§] and Kai Johnsson*[,†,‡,∥]

[†]École Polytechnique Fédérale de Lausanne, Institute of Chemical Sciences and Engineering, Lausanne CH-1015, Switzerland

[‡]National Centre of Competence in Research in Chemical Biology, Lausanne, CH-1015, Switzerland

[§]Novartis Institutes for BioMedical Research, Basel, CH-4056, Switzerland

[∥]Max-Planck-Institute for Medical Research, Department of Chemical Biology, 69120 Heidelberg, Germany

Supporting Information

**ABSTRACT:** We are introducing a new approach to evaluate cellular uptake of drugs and drug candidates into living cells. The approach is based on converting the protein target of a given class of compounds into a fluorescent biosensor. By measuring the binding of different compounds to their cognate biosensor in live cells and comparing these values to those measured in vitro, their cellular uptake and concentrations can be ranked. We demonstrate that our strategy enables the evaluation of the cellular uptake into the cytosol of 2 classes of inhibitors using two different sensor designs; first, sensors comprising the self-labeling protein SNAP conjugated with a chemically modified inhibitor shown for inhibitors of the enzyme human carbonic anhydrase II; and a label-free sensor for inhibitors of protein−protein interactions demonstrated for the protein pair p53−HDM2.

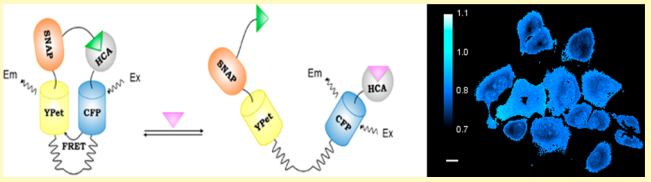


**KEYWORDS:** *intracellular concentration, FRET-based sensor protein, cellular absorption, cellular clearance, HCAII, p53-HDM2 interaction, peptide therapeutics*

Cellular uptake and membrane permeability are important determinants of the pharmacokinetic and pharmacodynamic properties of drugs and drug candidates. In addition, drug selectivity often depends on the presence or absence of specific transporters. A recent example that highlights the importance of (selective) drug uptake in pharmacology is the absolute dependency of the efficacy of the anticancer agent YM155 on the presence of a single solute carrier protein overexpressed in cancer cells.[1] The importance of drug uptake and permeability for drug research has been known for decades and there are also increased efforts to characterize the involved transporters,[2] yet there is a shortage of suitable assays to measure drug concentrations in live cells with spatiotemporal resolution. Several medium- to high-throughput scalable in vitro models are available to evaluate cellular uptake and membrane permeability. The most popular and widely used non-cell-based technique to estimate passive permeability is the Parallel Artificial Membrane Permeability Assay (PAMPA).[3−5] In PAMPA the cellular membrane is usually mimicked by a thin hexadecane layer on a filter plate that separates donor and acceptor reservoirs, allowing measurement of apparent permeability ($P_{app}$). Similar methods also exist for cell-based assays, where the artificial membrane has been replaced by monolayers of Madin Darby Canine Kidney (MDCK) or Caco-2 cells.[6,7] Such assays are valuable for investigating both passive and active permeation mechanisms as the cellular membranes contain transporters and pumps. However, these cell-based assays only provide information about the ability of a molecule to cross a cell layer and do not enable a direct evaluation of the molecule's cellular uptake. Approaches based on mass spectrometry or radioactively labeled drugs lack spatiotemporal resolution. As a complementary strategy to evaluate cellular uptake of drugs and drug candidates here we used Förster resonance energy transfer (FRET)-based ratiometric biosensors for in cellulo measurements of drug concentrations (Figure 1). Our sensor proteins are composed

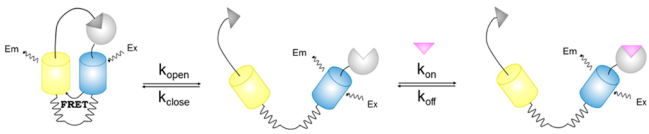


**Figure 1.** Design principle of the FRET sensor proteins to evaluate cellular uptake of drugs and drug candidates. The dark gray triangle represents a labeled SNAP-tag or a peptide, and the pink triangle the competing analyte. The yellow and blue cylinders represent YPet and CFP, respectively.

of the protein target of a drug (i.e., the drug target), two fluorescent proteins capable of FRET, and a ligand binding to the drug target. In the absence of the drug, intramolecular binding of the ligand to the drug target results in increased proximity of the two fluorescent proteins and a subsequent increase in FRET. In the presence of sufficiently high concentrations of the drug, the drug displaces the ligand from the drug target resulting in a

**Received:** May 18, 2017
**Accepted:** July 12, 2017




DOI: 10.1021/acssensors.7b00331
*ACS Sens.* XXXX, XXX, XXX−XXX

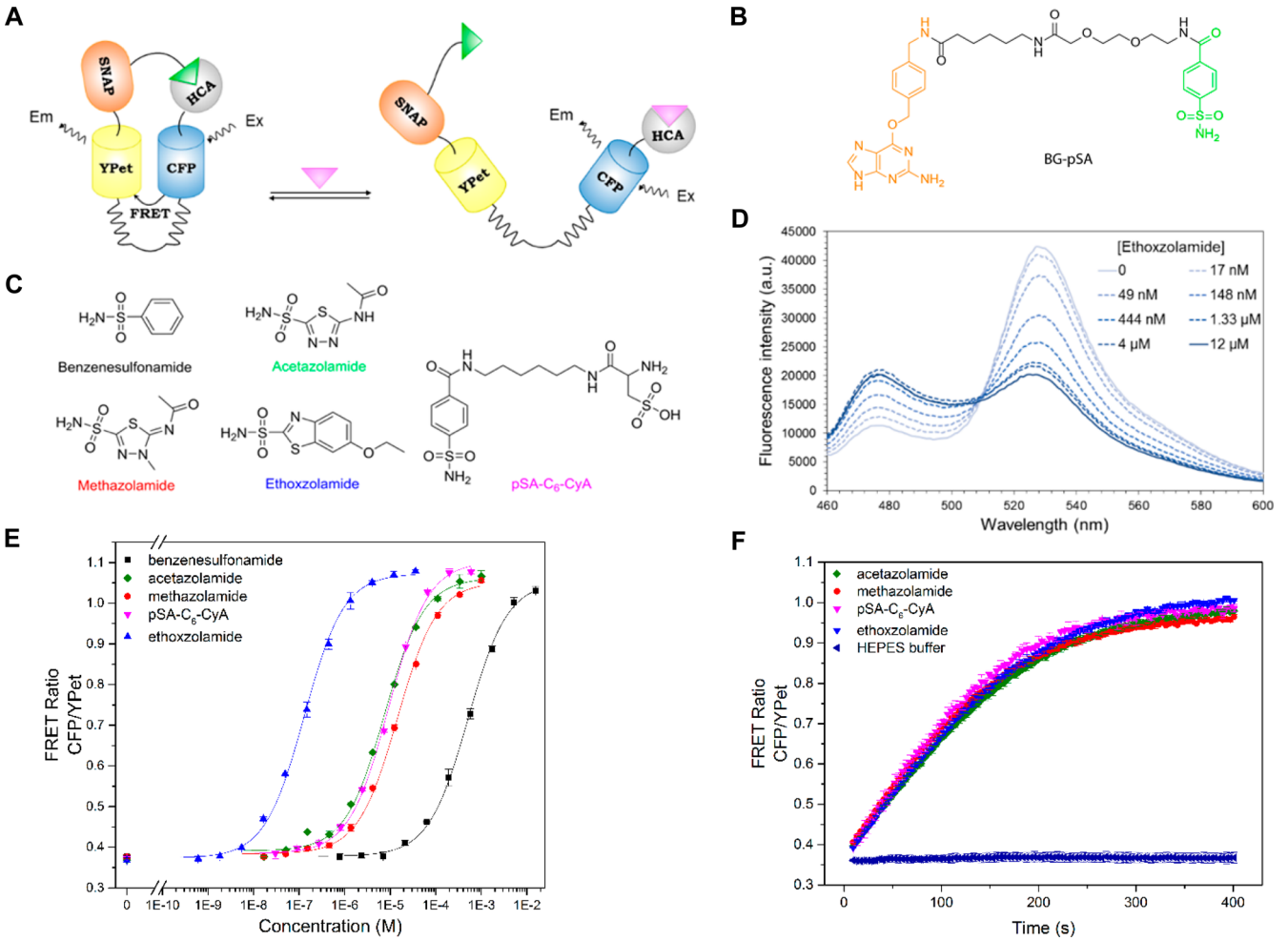


**Figure 2.** (A) Design of the HCAII-based sensor. The fusion protein SNAP-YPet-$Pro_{15}(GGS)_2Pro_{15}$-CFP-HCA is labeled with a synthetic molecule containing an HCAII intramolecular ligand (green triangle). Free analyte in solution (pink triangle) displaces the intramolecular ligand and shifts the sensor to the open conformation, consequently reducing FRET efficiency. (B) Structure of the synthetic molecule used to label the SNAP-tag moiety on the sensor. Benzylguanine (BG, in orange) and the HCAII inhibitor *para*-benzenesulfonamide (in green) are connected by a $C_6$-$EG_2$ linker, to give BG-pSA. (C) Structure of the HCAII inhibitors used in the experiments. (D) Example of in vitro emission spectra of SNAP-YPet-$Pro_{15}(GGS)_2Pro_{15}$-CFP-HCA labeled with BG-pSA in the presence of defined concentrations of the HCAII inhibitor ethoxzolamide. (E) In vitro fluorescence titration curves of the HCAII inhibitors shown in (C) with the labeled sensor. Each plot shows the FRET ratio CFP/YPet emission against the concentration of inhibitor; the data were fitted to a single-site binding isotherm. (F) In vitro opening kinetic curves of the HCAII-based sensor labeled with compound BG-pSA.

decrease in FRET. Analysis of the FRET ratio thus enables reading of cellular drug concentrations with temporal resolution. We validate our approach by generating biosensors for inhibitors of an enzyme, Human Carbonic Anhydrase II (HCAII),[8−10] and for inhibitors of a protein−protein interaction, the one between the tumor suppressor p53 and its negative regulator Human Double Minute 2 (HDM2).[11,12] We demonstrate how these biosensors enable a simple real-time monitoring of cellular uptake of different classes of inhibitors.

## RESULTS AND DISCUSSION

**HCAII-Based Sensor Design and Sensing of HCAII Inhibitors In Vitro.** Human Carbonic Anhydrase II (HCAII) is an enzyme involved in many physiological processes and biosynthetic cascades (e.g., $CO_2$ transport, pH homeostasis, lipogenesis, ureagenesis, and gluconeogenesis). Inhibitors of HCAII are used as diuretics and for the treatment of glaucoma and epilepsy.[13,14] The most important class of HCA-inhibitors is represented by sulfonamides, many of which are already widespread therapeutics. To create a sensor for HCA inhibitors, we expressed HCAII as a fusion protein with the fluorescent proteins CFP and YPet,[15] and SNAP-tag[16,17] (Figure 2A). The fluorescent proteins are a good FRET pair and are separated by two flexible GGS repetitions[18] inserted between two 15-residue-long poly(L-proline) chains, known to fold into a rigid helical structure.[19] SNAP-tag is covalently labeled with a *para*-benzenesulfonamide benzylguanine derivative (BG-pSA, Figure 2B), and excess free BG-pSA is removed by washing. The tethered pSA binds to the active site of HCAII, maintaining the semisynthetic sensor in the closed conformation, where CFP and YPet are in close proximity and FRET is efficient. Addition of free HCAII inhibitor, the analyte, displaces the internal ligand from the receptor protein, while the semirigid GGS/proline-based linker ensures significant distancing between CFP and YPet with a consequent drop in FRET efficiency. The variation of FRET efficiency can be measured and correlated with the concentration of analyte at a given time point. Conceptually, the present sensor design is similar to our previous HCA-based sensors based on the SNIFIT concept.[20,21] However, in our previous work, the tethered ligand also contained a fluorophore as part of the linker,


DOI: 10.1021/acssensors.7b00331
ACS Sens. XXXX, XXX, XXX−XXX

**Table 1. Comparison between the In Vitro and In Cellulo $c_{50}$ Values, and between the In Vitro and In Cellulo $k_{open}$ of the HCAII Inhibitors**

| inhibitor | $c_{50}$ in vitro ($\mu$M) | $c_{50}$ in cellulo ($\mu$M) | $k_{open}$ in vitro ($\times 10^{-3}$ s$^{-1}$) | $k_{open}$[a] in cellulo ($\times 10^{-3}$ s$^{-1}$) |
|---|---|---|---|---|
| benzenesulfonamide | 500 ± 50 | 760 ± 58 | 13.2 ± 0.1 | 13.6 ± 0.9 |
| acetazolamide | 7.3 ± 0.5 | 9.5 ± 0.7 | 10.7 ± 0.1 | 10.1 ± 0.6 |
| methazolamide | 14.1 ± 0.9 | 17.7 ± 1.4 | 12.0 ± 0.1 | 13.9 ± 0.7 |
| pSA-$C_6$-CyA | 8.9 ± 0.5 | >1 mM | 13.2 ± 0.1 | <0.18 ± 0.02[b] |
| ethoxzolamide | 0.170 ± 0.014 | 0.078 ± 0.006 | 10.7 ± 0.1 | 11.4 ± 0.4 |

[a]Apparent $k_{open}$. [b]The change in FRET ratio for pSA-$C_6$-CyA is similar to that of buffer.

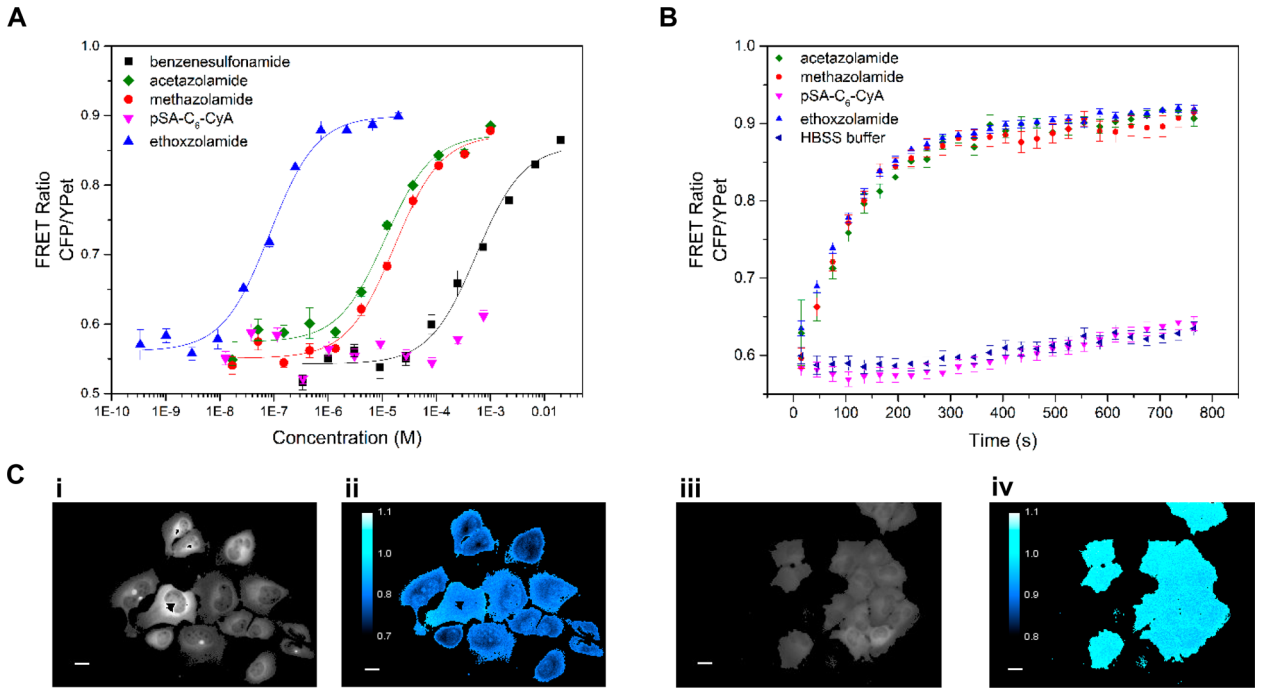


**Figure 3.** (A) In cellulo (U2OS cells) fluorescence titration curves of the HCAII inhibitors with the labeled sensor. Each plot shows the ratio CFP/YPet emission against the concentration of inhibitor; the data were fitted to a single-site binding isotherm. (B) In cellulo (U2OS cells) opening kinetic curves of the HCAII-based sensor labeled with compound BG-pSA. (C) U2OS cells expressing the HCAII-based sensor: (i) YPet (FRET) channel emission image and (ii) FRET ratio image of the cells in absence of acetazolamide; (iii) YPet (FRET) channel emission image and (iv) FRET ratio image of the cells at equilibrium with acetazolamide 300 $\mu$M. Scale bars, 20 $\mu$m.

rendering the molecule membrane impermeable and not suitable for intracellular applications.[21] In contrast, overnight incubation of U2OS cells expressing SNAP-tag with BG-pSA (5 $\mu$M) resulted in quantitative labeling of SNAP-tag (Figure S6), opening up the way for intracellular applications of our HCA sensor.

The HCA sensor, purified from HEK 293 cells (Figure S1) and labeled with BG-pSA, was characterized in vitro. Incubation of the sensor with increasing concentrations of the approved drug ethoxzolamide (Ethamide, Figure 2C) reduced FRET efficiency between CFP and YPet and resulted in a 3- to 4-fold FRET ratio change (Figure 2D,E). The $c_{50}$ of ethoxzolamide, which corresponds to the concentration of inhibitor that leads to the half-maximal FRET ratio change, was measured to be 160 nM (Table 1). This value is 40 times higher than its reported $K_D$ of 4 nM, the difference being due to the competition between free ethoxzolamide and tethered benzenesulfonamide. We repeated these titration experiments in vitro with other HCAII inhibitors: two additional marketed drugs, i.e., acetazolamide (Diamox) and methazolamide (Neptazane), benzenesulfonamide, and a *para*-benzenesulfonamide derivative linked to cysteic acid (pSA-$C_6$–CyA). The latter compound was synthesized in order to have a compound with predicted low cellular uptake; we assumed that the permanently charged cysteic acid (p$K_a$ = 1.3[22]) would render this molecule impermeable. For each compound, we determined the $c_{50}$ value (Table 1). In these measurements, benzenesulfonamide had the highest $c_{50}$ of 550 $\mu$M, while the $c_{50}$ values of acetazolamide, methazolamide, and pSA-$C_6$-CyA were all around 10 $\mu$M. The $c_{50}$ values cannot be compared directly to published $K_D$ values, but they reflect the relative affinities of these compounds: the published $K_D$ of benzenesulfonamide is 72-fold higher than that of acetazolamide,[8,23] and its $c_{50}$ value is 70-fold higher. For a given sensor, $c_{50}$ values thus can be used to rank inhibitors according to their affinities.

We then characterized the sensor kinetics in vitro, which will be important for an analysis of cellular uptake of HCAII inhibitors. In these measurements, we followed the FRET ratio change as a function of time and fitted the kinetics to an exponential function yielding an apparent rate constant $k_{open}$, assuming "irreversible" sensor opening due to large excess of inhibitor. For the in vitro experiments, the inhibitors were added to the labeled sensor at concentrations well above their respective $c_{50}$ values and the kinetics of the opening of the sensor was recorded (Figure 2F, Table S1). For all five HCAII inhibitors the


DOI: 10.1021/acssensors.7b00331
ACS Sens. XXXX, XXX, XXX−XXX

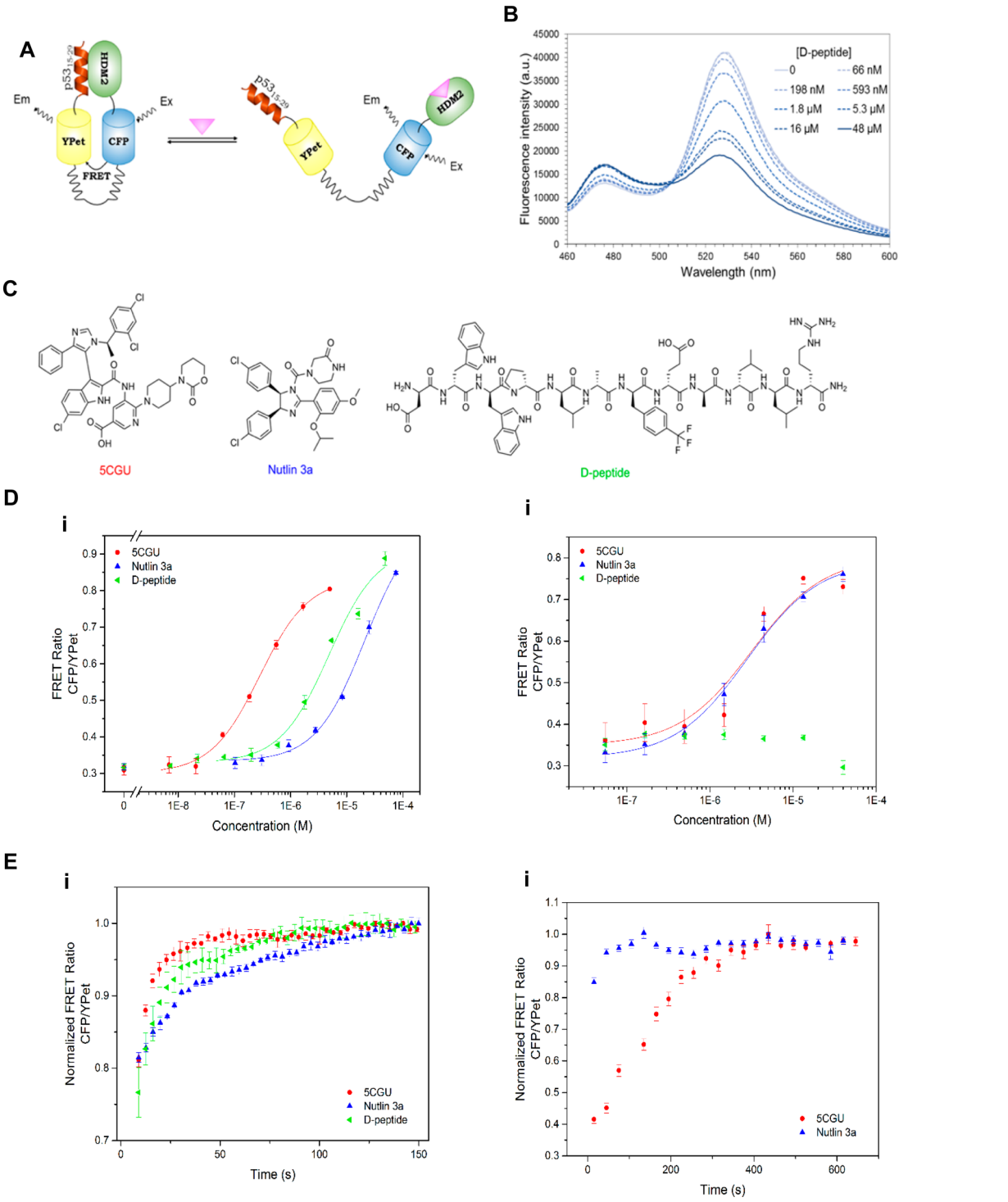


**Figure 4.** (A) Design of the label-free p53-HDM2-PPI biosensor, constituted by the fusion protein $p53_{15-29}$-YPet-$Pro_{15}(GGS)_2Pro_{15}$-CFP-$HDM2_{17-125}$. Free analyte in solution (pink triangle) displaces the p53-peptide intramolecular ligand and shifts the sensor to the open conformation, consequently reducing the FRET efficiency. (B) Example of in vitro emission spectra of the p53-based sensor in the presence of defined concentrations of the inhibitor D-peptide. (C) Structure of the inhibitors of the p53-HDM2 interaction used in the experiments. (D) (i) In vitro and (ii) in cellulo (U2OS cells) fluorescence titration curves of the inhibitors shown in (C) with the p53-based sensor. (E) (i) In vitro opening kinetic curves of the p53-based sensor with the inhibitors shown in (C); (ii) in cellulo (U2OS cells) opening kinetic curves with the cell permeable 5CGU and Nutlin 3a, both applied at 100 $\mu$M.

kinetics of opening was monoexponential and the corresponding rate constants $k_{open}$ for all five inhibitors were virtually identical (Table 1). These data suggest that the rate of opening is governed by the unbinding of the tethered ligand, as previously observed for other SNIFITS.[21,24,25]

**Evaluating Cellular Uptake of HCAII Inhibitors.** We expressed the HCAII sensor in the cytosol of U2OS cells and labeled SNAP-tag with BG-pSA (overnight incubation with 5 $\mu$M BG-pSA). After labeling, cells were washed to remove free pBG-SA and incubated with increasing concentrations of the different



DOI: 10.1021/acssensors.7b00331
ACS Sens. XXXX, XXX, XXX−XXX

inhibitors. After an incubation period of 60 min, we measured the intracellular sensor response to the varying concentrations of the inhibitors by automated fluorescence microscopy and determined average FRET ratios per group of cells (Figure 3A,B and Figure 2S). The obtained FRET ratios were then plotted as a function of inhibitor concentrations. Compared to the values obtained in vitro, the in cellulo use of the sensor provoked a loss of FRET ratio dynamic range from about 3−4-fold to about 1.7-fold (cf., Figure 2E and Figure 3A). We attribute this effect to the reduction of signal-to-noise ratio (SNR) due to background autofluorescence of biological samples.[26,27] Nevertheless, the HCAII-based sensor exhibited a dynamic range sufficiently wide to allow accurate measurements of in cellulo $c_{50}$ values (Figure 3A, Table 1). Remarkably, the $c_{50}$ values for ethoxzolamide, acetazolamide, methazolamide, and benzenesulfonamide determined in vitro and in cellulo were rather similar (within a factor of 2). This result suggests that in U2OS cells these simple sulfonamides do not depend on active transport to enter the cytosol of the cells and are also not actively pumped out of the cytosol of U2OS cells, since the presence of active influx or efflux would have shifted the $c_{50}$ values to lower or higher concentrations, respectively. In contrast, incubation of U2OS cells with pSA-$C_6$-CyA at concentrations significantly above its in vitro $c_{50}$ value only resulted in minor FRET ratio changes. This suggests that pSA-$C_6$-CyA does not enter the cytosol of cells or that it is a substrate of efflux pumps.

We then evaluated the in cellulo kinetic response of the HCAII-based in the cytosol of U2OS in 96-well plates. Following the addition of the inhibitor of interest at the same concentrations as for the in vitro kinetic experiments, cells were immediately imaged by fluorescence microscopy over time as described above. The experiments in cellulo showed that the opening kinetics of the intracellular sensor for ethoxzolamide, acetazolamide, methazolamide, and benzenesulfonamide were indistinguishable and comparable to the values obtained in the in vitro experiments (Figure 3C, Table 1). This indicates that for these four compounds uptake into the cytosol of U2OS cells is faster than the kinetics of sensor opening. In contrast (and as expected), addition of pSA-$C_6$-CyA did not result in a significant change of FRET ratio.

**Intracellular Sensing of p53-HDM2 Inhibitors with a Label-Free Sensor.** We then attempted to apply our approach to inhibitors of protein−protein interactions (PPIs). One of the most notorious PPIs in cancer biology is the one between the tumor suppressor p53 and its negative regulator Human Double Minute 2 (HDM2).[11,12] Inhibition of the interaction between p53 and HDM2 prevents the degradation of p53 and several small molecules and peptidic inhibitors of this interaction are currently undergoing clinical trials for the treatment of human cancers.[28−30] The sensor for inhibitors of the interaction p53-HDM2 follows the general design principle of Figure 1. The protein target is the HDM2 fragment $HDM2_{17-125}$ and the intramolecular ligand the p53-derived peptide $p53_{15-29}$ (Figure 4A). Crystallographic analysis revealed that these two fragments mediate the interaction of the two proteins.[31] Our p53-HDM2-PPI biosensor then had the following sequence: $p53_{15-29}$-YPet-$Pro_{15}(GGS)_2Pro_{15}$-CFP-$HDM2_{17-125}$. The sensor can be entirely genetically encoded and no labeling is required to render it functional. Other fluorescence-based biosensors for monitoring the p53-HDM2 interaction have been introduced previously.[32,33] However, these biosensors are based on two different components, which makes the readout dependent on the relative stoichiometry and absolute concentration of the components, thereby complicating quantifications.

We purified the p53-HDM2-PPI sensor protein from HEK 293 cells (Figure S3) and characterized its interaction with three different classes of inhibitors of the p53-HDM2 interaction (Figure 4C): the first one is Nutlin 3a, which was the first example of a small-molecule inhibitor of this PPI.[34] It is effective in killing wildtype p53 cancer cells, but its toxicity and poor pharmacokinetics has prevented its use in the clinic.[28] The second compound is the imidazole derivative 5CGU, which was prepared according to published procedures.[35] This compound shows quite good solubility and is related to a derivative currently in clinical trials.[36] The third compound is a fluorinated derivative of the previously reported D-peptide $^{D}PMI_{\gamma}$,[37] which was obtained by standard solid phase peptide synthesis. This particular HDM2-binder, derived from an optimization on the basis of mirror-image phage display, was chosen due to its stability and high affinity for the target. Incubation of the p53-HDM2-PPI sensor with increasing concentrations of inhibitor resulted in decrease of FRET efficiency, resulting in a maximum 2.6−2.9-fold FRET ratio increase (Figure 4B). The measured $c_{50}$ values of the three inhibitors increase in the order 5CGU < D-peptide < Nutlin 3a (Figure 4D, Table 2), which is in agreement with the literature $K_D$ values for these inhibitors.[34,35] We then measured the rate of opening of the p53-HDM2-PPI sensor upon addition of the inhibitors at concentrations above their $c_{50}$ values. In these experiments, all three inhibitors displayed nearly identical rate constants $k_{open}$ of about $(7-9) \times 10^{-2}$ $s^{-1}$. We assume that, as for the HCA sensor, unbinding of the intramolecular ligand is rate-determining.

**Table 2. Comparison between the In Vitro and In Cellulo $c_{50}$ Values, and between the In Vitro and In Cellulo $k_{open}$ of of the Inhibitors of the p53-HDM2 Interaction**

| inhibitor | $c_{50}$ in vitro ($\mu$M) | $c_{50}$ in cellulo ($\mu$M) | $k_{open}$ in vitro ($\times 10^{-3}$ $s^{-1}$) | $k_{open}$[a] in cellulo ($\times 10^{-3}$ $s^{-1}$) |
|---|---|---|---|---|
| 5CGU | 0.29 ± 0.03 | 2.2 ± 0.6 | 99.2 ± 3.9 | 6.9 ± 0.4 |
| Nutlin 3a | 23.2 ± 1.4 | 3.0 ± 0.8 | 72.0 ± 1.7 | 125 ± 9 |
| D-peptide | 3.7 ± 0.3 | n.d. | 76.9 ± 5.3 | n.d. |

[a]Apparent $k_{open}$.

We then expressed the sensor in the cytosol of U2OS cells (Figure S4) and determined both $c_{50}$ values and rate constants $k_{open}$ of sensor opening for the three inhibitors. Interestingly, the order of the $c_{50}$ values was the opposite of that measured in vitro: the $c_{50}$ value of Nutlin 3a decreased about 10-fold, whereas the $c_{50}$ value of 5CGU increased about 10-fold. The latter finding can be explained by the presence of the carboxylic acid function, which limits permeability of 5CGU. In a recent study on cellular activity of 5CGU and related derivatives, this particular compound also showed only a weak cellular potency.[38] For the D-peptide, no $c_{50}$ value could be obtained, indicating that this peptide did not access the cytosol of U2OS cells, or is subject to effective efflux. In addition, the kinetic experiment on the cell line revealed that 5CGU enters the cells significantly slower than Nutlin 3a when the two compounds are applied at the same concentration (100 $\mu$M, Figure 4D iii, Table 2). The in cellulo titration and kinetic measurements suggest that the intracellular concentrations of 5CGU and Nutlin 3a are influenced by active transport mechanisms (efflux and influx pumps, respectively). In particular, since dose-dependent inhibition of an ABC-transporter activity


DOI: 10.1021/acssensors.7b00331
ACS Sens. XXXX, XXX, XXX−XXX

has been described for Nutlin-3a,[39] we cannot rule out a differential influence of this class of transporters on Nutlin-3a and 5CGU. For this reason, general molecular comparisons regarding permeability should be accompanied by an assessment of transporter activity.

## CONCLUSIONS

We have demonstrated how FRET-based biosensors can be utilized to evaluate cellular uptake of drugs and drug candidates with temporal resolution in live cells, and in a label-free manner for sensors of PPI inhibitors. Organelle specific targeting of the genetically encoded sensors should allow measurement of luminal analyte concentrations. We generated biosensors for two classes of clinically relevant compounds, inhibitors of the enzyme HCAII and inhibitors of the protein−protein interaction p53-HDM2. Compounds belonging to the same family could be compared with respect to their ability to access the cytosol. As a result of this study, efficient intracellular sensing can be realized using this type of fusion protein either by conjugation of small molecule binders via the SNAP-tag technology or, if available, by considering fusions with natural peptide or protein binders, which do not require further modification. Although not exemplified in this set of experiments, the properties of an HDM2 sensor based on a peptide could possibly be compared to the corresponding construct modified with a small molecule to show superiority for one or the other approach. The modular design of our biosensors lends itself to potentially be adapted to the detection of other families of molecules, assisting their pharmaceutical profiling, and should aid in the design of improved variants.

## ASSOCIATED CONTENT

### Supporting Information

The Supporting Information is available free of charge on the ACS Publications website at DOI: 10.1021/acssensors.7b00331.

Additional figures and tables, protocols of chemical synthesis and of biochemical and cellular assays (PDF)

## AUTHOR INFORMATION


### Corresponding Author

*E-mail: kai.johnsson@mpimf-heidelberg.mpg.de.

### ORCID

Kui Thong Tan: 0000-0002-0091-8546

Ruud Hovius: 0000-0001-9258-6587

Kai Johnsson: 0000-0002-8002-1981

### Present Addresses

[#]National Tsing Hua University, Department of Chemistry, Hsinchu, Taiwan.

[¶]Lucentix SA, EPFL Innovation Park, Lausanne, Switzerland.


### Author Contributions

All authors contributed to the design of the experiments. S.S., K.T.T., R.G., and P.L.D.A. performed the experiments. All authors contributed to the interpretation of the data and the writing of the manuscript. All authors have given approval to the final version of the manuscript.

### Notes

The authors declare no competing financial interest.

## ACKNOWLEDGMENTS

This work was supported by École Polytechnique Fédérale de Lausanne, and the National Centre of Competence in Research Chemical Biology. We are grateful to Luc Patiny for the help in establishing the protocol for image analysis and to Roman Wille for technical assistance.

## REFERENCES


(1) Winter, G. E.; Radic, B.; Mayor-Ruiz, C.; Blomen, V. A.; Trefzer, C.; Kandasamy, R. K.; Huber, K. V.; Gridling, M.; Chen, D.; Klampfl, T.; Kralovics, R.; Kubicek, S.; Fernandez-Capetillo, O.; Brummelkamp, T. R.; Superti-Furga, G. The solute carrier SLC35F2 enables YM155-mediated DNA damage toxicity. *Nat. Chem. Biol.* **2014**, *10* (9), 768−773.

(2) Cesar-Razquin, A.; Snijder, B.; Frappier-Brinton, T.; Isserlin, R.; Gyimesi, G.; Bai, X.; Reithmeier, R. A.; Hepworth, D.; Hediger, M. A.; Edwards, A. M.; Superti-Furga, G. A Call for Systematic Research on Solute Carriers. *Cell* **2015**, *162* (3), 478−487.

(3) Kansy, M.; Senner, F.; Gubernator, K. Physicochemical high throughput screening: parallel artificial membrane permeation assay in the description of passive absorption processes. *J. Med. Chem.* **1998**, *41* (7), 1007−1010.

(4) Avdeef, A.; Bendels, S.; Di, L.; Faller, B.; Kansy, M.; Sugano, K.; Yamauchi, Y. PAMPA−critical factors for better predictions of absorption. *J. Pharm. Sci.* **2007**, *96* (11), 2893−2909.

(5) Avdeef, A.; Tsinman, O. PAMPA–a drug absorption in vitro model 13. Chemical selectivity due to membrane hydrogen bonding: in combo comparisons of HDM-, DOPC-, and DS-PAMPA models. *Eur. J. Pharm. Sci.* **2006**, *28* (1−2), 43−50.

(6) Irvine, J. D.; Takahashi, L.; Lockhart, K.; Cheong, J.; Tolan, J. W.; Selick, H. E.; Grove, J. R. MDCK (Madin-Darby canine kidney) cells: A tool for membrane permeability screening. *J. Pharm. Sci.* **1999**, *88* (1), 28−33.

(7) Braun, A.; Hämmerle, S.; Suda, K.; Rothen-Rutishauser, B.; Günthert, M.; Krämer, S. D.; Wunderli-Allenspach, H. Cell cultures as tools in biopharmacy. *Eur. J. Pharm. Sci.* **2000**, *11*, S51−S60.

(8) Krishnamurthy, V. M.; Kaufman, G. K.; Urbach, A. R.; Gitlin, I.; Gudiksen, K. L.; Weibel, D. B.; Whitesides, G. M. Carbonic anhydrase as a model for biophysical and physical-organic studies of proteins and protein-ligand binding. *Chem. Rev.* **2008**, *108* (3), 946−1051.

(9) Innocenti, A.; Firnges, M. A.; Antel, J.; Wurl, M.; Scozzafava, A.; Supuran, C. T. Carbonic anhydrase inhibitors. Inhibition of the membrane-bound human and bovine isozymes IV with sulfonamides. *Bioorg. Med. Chem. Lett.* **2005**, *15* (4), 1149−1154.

(10) Esbaugh, A. J.; Tufts, B. L. The structure and function of carbonic anhydrase isozymes in the respiratory system of vertebrates. *Respir. Physiol. Neurobiol.* **2006**, *154* (1−2), 185−198.

(11) Liang, Y.; Liu, J.; Feng, Z. The regulation of cellular metabolism by tumor suppressor p53. *Cell Biosci.* **2013**, *3* (1), 9.

(12) Hollstein, M.; Sidransky, D.; Vogelstein, B.; Harris, C. p53 mutations in human cancers. *Science* **1991**, *253* (5015), 49−53.

(13) Supuran, C. T. Carbonic anhydrases: novel therapeutic applications for inhibitors and activators. *Nat. Rev. Drug Discovery* **2008**, *7* (2), 168−181.

(14) Supuran, C. T.; Scozzafava, A. Carbonic anhydrases as targets for medicinal chemistry. *Bioorg. Med. Chem.* **2007**, *15* (13), 4336−4350.

(15) Kremers, G. J.; Goedhart, J.; van Munster, E. B.; Gadella, T. W., Jr. Cyan and yellow super fluorescent proteins with improved brightness, protein folding, and FRET Forster radius. *Biochemistry* **2006**, *45* (21), 6570−6580.

(16) Keppler, A.; Gendreizig, S.; Gronemeyer, T.; Pick, H.; Vogel, H.; Johnsson, K. A general method for the covalent labeling of fusion proteins with small molecules in vivo. *Nat. Biotechnol.* **2002**, *21* (1), 86−89.

(17) Juillerat, A.; Gronemeyer, T.; Keppler, A.; Gendreizig, S.; Pick, H.; Vogel, H.; Johnsson, K. Directed evolution of O6-alkylguanine-DNA alkyltransferase for efficient labeling of fusion proteins with small molecules in vivo. *Chem. Biol.* **2003**, *10* (4), 313−317.

(18) Evers, T. H.; van Dongen, E. M.; Faesen, A. C.; Meijer, E. W.; Merkx, M. Quantitative understanding of the energy transfer between




DOI: 10.1021/acssensors.7b00331
ACS Sens. XXXX, XXX, XXX−XXX

fluorescent proteins connected via flexible peptide linkers. *Biochemistry* **2006**, *45* (44), 13183−13192.
(19) Arora, P. S.; Ansari, A. Z.; Best, T. P.; Ptashne, M.; Dervan, P. B. Design of Artificial Transcriptional Activators with Rigid Poly-l-proline Linkers. *J. Am. Chem. Soc.* **2002**, *124* (44), 13067−13071.
(20) Brun, M. A.; Tan, K. T.; Nakata, E.; Hinner, M. J.; Johnsson, K. Semisynthetic fluorescent sensor proteins based on self-labeling protein tags. *J. Am. Chem. Soc.* **2009**, *131* (16), 5873−5884.
(21) Brun, M. A.; Griss, R.; Reymond, L.; Tan, K. T.; Piguet, J.; Peters, R. J.; Vogel, H.; Johnsson, K. Semisynthesis of fluorescent metabolite sensors on cell surfaces. *J. Am. Chem. Soc.* **2011**, *133* (40), 16235−16242.
(22) Enami, S.; Hoffmann, M. R.; Colussi, A. J. Ozone oxidizes glutathione to a sulfonic acid. *Chem. Res. Toxicol.* **2009**, *22* (1), 35−40.
(23) Barrese, A. A. I. High-Throughput Screening Studies of Inhibition of Human Carbonic Anhydrase II and Bacterial Flagella Antimicrobial Activity; *Western Michigan University Dissertations*, 2010; Paper 500.
(24) Masharina, A.; Reymond, L.; Maurel, D.; Umezawa, K.; Johnsson, K. A fluorescent sensor for GABA and synthetic GABA(B) receptor ligands. *J. Am. Chem. Soc.* **2012**, *134* (46), 19026−19034.
(25) Brun, M. A.; Tan, K. T.; Griss, R.; Kielkowska, A.; Reymond, L.; Johnsson, K. A semisynthetic fluorescent sensor protein for glutamate. *J. Am. Chem. Soc.* **2012**, *134* (18), 7676−7678.
(26) Ettinger, A.; Wittmann, T. Fluorescence live cell imaging. *Methods Cell Biol.* **2014**, *123*, 77−94.
(27) Waters, J. C. Accuracy and precision in quantitative fluorescence microscopy. *J. Cell Biol.* **2009**, *185* (7), 1135−1148.
(28) Burgess, A.; Chia, K. M.; Haupt, S.; Thomas, D.; Haupt, Y.; Lim, E. Clinical Overview of MDM2/X-Targeted Therapies. *Front. Oncol.* **2016**, *6*, 7.
(29) Vu, B.; Wovkulich, P.; Pizzolato, G.; Lovey, A.; Ding, Q.; Jiang, N.; Liu, J. J.; Zhao, C.; Glenn, K.; Wen, Y.; Tovar, C.; Packman, K.; Vassilev, L.; Graves, B. Discovery of RG7112: A Small-Molecule MDM2 Inhibitor in Clinical Development. *ACS Med. Chem. Lett.* **2013**, *4* (5), 466−469.
(30) Andreeff, M.; Kelly, K. R.; Yee, K.; Assouline, S.; Strair, R.; Popplewell, L.; Bowen, D.; Martinelli, G.; Drummond, M. W.; Vyas, P.; Kirschbaum, M.; Iyer, S. P.; Ruvolo, V.; Gonzalez, G. M.; Huang, X.; Chen, G.; Graves, B.; Blotner, S.; Bridge, P.; Jukofsky, L.; Middleton, S.; Reckner, M.; Rueger, R.; Zhi, J.; Nichols, G.; Kojima, K. Results of the Phase I Trial of RG7112, a Small-Molecule MDM2 Antagonist in Leukemia. *Clin. Cancer Res.* **2016**, *22* (4), 868−876.
(31) Kussie, P. H.; Gorina, S.; Marechal, V.; Elenbaas, B.; Moreau, J.; Levine, A. J.; Pavletich, N. P. Structure of the MDM2 Oncoprotein Bound to the p53 Tumor Suppressor Transactivation Domain. *Science* **1996**, *274* (5289), 948−953.
(32) Herce, H. D.; Deng, W.; Helma, J.; Leonhardt, H.; Cardoso, M. C. Visualization and targeted disruption of protein interactions in living cells. *Nat. Commun.* **2013**, *4*, 2660.
(33) Dudgeon, D. D.; Shinde, S. N.; Shun, T. Y.; Lazo, J. S.; Strock, C. J.; Giuliano, K. A.; Taylor, D. L.; Johnston, P. A.; Johnston, P. A. Characterization and optimization of a novel protein-protein interaction biosensor high-content screening assay to identify disruptors of the interactions between p53 and hDM2. *Assay Drug Dev. Technol.* **2010**, *8* (4), 437−458.
(34) Vassilev, L. T.; Vu, B. T.; Graves, B.; Carvajal, D.; Podlaski, F.; Filipovic, Z.; Kong, N.; Kammlott, U.; Lukacs, C.; Klein, C.; Fotouhi, N.; Liu, E. A. In vivo activation of the p53 pathway by small-molecule antagonists of MDM2. *Science* **2004**, *303* (5659), 844−848.
(35) Furet, P.; Kallen, J.; Lorber, J.; Masuya, K.; Novartis, AG. International Patent No. WO2012176123A1 2012.
(36) Jeay, S.; Gaulis, S.; Ferretti, S.; Bitter, H.; Ito, M.; Valat, T.; Murakami, M.; Ruetz, S.; Guthy, D. A.; Rynn, C.; Jensen, M. R.; Wiesmann, M.; Kallen, J.; Furet, P.; Gessier, F.; Holzer, P.; Masuya, K.; Würthner, J.; Halilovic, E.; Hofmann, F.; Sellers, W. R.; Graus Porta, D. A distinct p53 target gene set predicts for response to the selective p53−HDM2 inhibitor NVP-CGM097. *eLife* **2015**, *4*, e06498.
(37) Liu, M.; Li, C.; Pazgier, M.; Li, C.; Mao, Y.; Lv, Y.; Gu, B.; Wei, G.; Yuan, W.; Zhan, C.; Lu, W. Y.; Lu, W. D-peptide inhibitors of the p53-MDM2 interaction for targeted molecular therapy of malignant neoplasms. *Proc. Natl. Acad. Sci. U. S. A.* **2010**, *107* (32), 14321−14326.
(38) D'Alessandro, P. L.; Buschmann, N.; Kaufmann, M.; Furet, P.; Baysang, F.; Brunner, R.; Marzinzik, A.; Vorherr, T.; Stachyra, T. M.; Ottl, J.; Lizos, D. E.; Cobos-Correa, A. Bioorthogonal Probes for the Study of MDM2-p53 Inhibitors in Cells and Development of High Content Screening Assays for Drug Discovery. *Angew. Chem., Int. Ed.* **2016**, *55*, 16026.
(39) Zhang, F.; Throm, S. L.; Murley, L. L.; Miller, L. A.; Zatechka, D. S.; Guy, R. K.; Kennedy, R.; Stewart, C. F. MDM2 antagonist nutlin-3a reverses mitoxantrone resistance by inhibiting breast cancer resistance protein mediated drug transport. *Biochem. Pharmacol.* **2011**, *82*, 24−34.


DOI: 10.1021/acssensors.7b00331
*ACS Sens.* XXXX, XXX, XXX−XXX